EurJIC
European Journal of Inorganic Chemistry

Full Papers
doi.org/10.1002/ejic.202100446

Chemistry Europe
European Chemical Societies Publishing

NON-Ligated *N*-Heterocyclic Tetrylenes

Felix Krämer,[a] Martin S. Luff,[b] Udo Radius,[b] Florian Weigend,[c] and Frank Breher*[a]

Dedicated to Prof. Hansgeorg Schnöckel on the occasion of his 80th birthday

We report on the synthesis of *N*-heterocyclic tetrylenes ligated by the NON-donor framework 4,5-bis(2,6-diisopropylphenylamino)-2,7-di-*tert*-butyl-9,9-dimethylxanthene. The molecular structures of the germylene (**3**), stannylene (**4**) and plumbylene (**5**) where determined by X-ray diffraction studies. Furthermore, we present quantum chemical studies on the σ-donor and π-acceptor properties of **3**–**5**. Additionally, we report on the reactivity of the tetrylenes towards the transition metal carbonyls $[Rh(CO)_2Cl]_2$, $[W(CO)_6]$ and $[Ni(CO)_4]$. The isolated complexes (**6** and **7**) show the differing reactivity of NHTs compared to NHCs. Instead of just forming the anticipated complex [(NON)Sn–$Rh(CO)_2$Cl], **4** inserts into the Rh–Cl bond to afford [(NON)Sn(Cl)Rh(CO)(C_6H_6)] (**6**, additional CO/C_6H_6 exchange) and [(NON)Sn(Cl)$Rh_2(CO)_4$Cl] (**7**). By avoiding halogenated transition metal precursors in order to prevent insertion reactions, germylene **3** shows "classical" coordination chemistry towards {$Ni(CO)_3$} forming the complex [(NON)Ge–$Ni(CO)_3$] (**8**).

Introduction

N-heterocyclic carbenes (NHCs) and their transition metal complexes have been extensively studied within the past 30 years. They have found application in catalysis as well as in medical, luminescent and functional materials.[1] However, various efforts have been made to modify the electronic and steric properties of NHCs by varying the ring-size, the substituent pattern or the composition of the *N*-heterocyclic backbone.[2]

N-heterocyclic tetrylenes (NHTs), i.e. the heavier analogs of NHCs, contain a divalent group 14 element (Scheme 1). Due to their great potential in many fields of organometallic and coordination chemistry, NHTs have been frequently reviewed.[3] One key feature of these ligands is their Lewis-amphoteric character. In their electronic ground-state, they possess an s-type donor orbital (lone pair) and a vacant p orbital serving as acceptor orbital.[3b,4] One difference to NHCs is that NHTs are weaker σ-donors and stronger π-acceptors.[5] Their electron donating capacity thus decreases upon descending the group 14.[6]

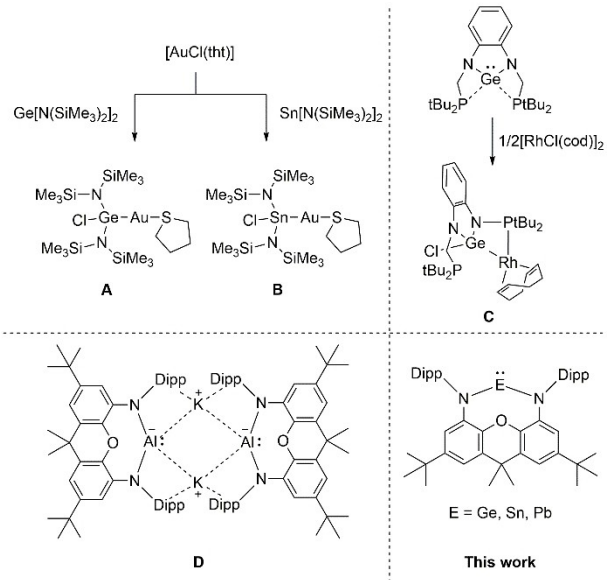

Scheme 1. Selected examples of insertion of tetrylenes into transition metal chlorine bonds and NON compounds.

The coordination chemistry of *N*-heterocyclic tetrylenes has developed remarkably since their first report.[7] Transition metal complexes bearing NHSi and NHGe as ligands were applied in catalysis by the group of Driess.[7i,8] Theoretical studies by the group of Szilvási showed that several *N*-heterocyclic silylenes and germylenes can compete or even outperform "classical" ligands such as carbenes and phosphines in relevant properties like σ-donor and π-acceptor strength, ligand-to-metal charge transfer and steric properties.[9] Khan, Pati and Jones showed that *N*-heterocyclic germylenes and stannylenes even catalyze cyanosilylation and hydroboration of aldehydes by themselves.[10] A rare example for the application of an *N*-

[a] F. Krämer, Prof. Dr. F. Breher
Karlsruhe Institute of Technology
Institute of Inorganic Chemistry
Engesserstraße 15, 76131 Karlsruhe, Germany
E-mail: breher@kit.edu
https://www.aoc.kit.edu/breher/index.php
[b] M. S. Luff, Prof. Dr. U. Radius
Julius-Maximilians-Universität Würzburg
Institute of Inorganic Chemistry
Am Hubland, 97074 Würzburg, Germany
[c] Prof. Dr. F. Weigend
Philipps-Universität Marburg
Department of Chemistry
Hans-Meerwein-Straße 4, 35032 Marburg, Germany

Supporting information for this article is available on the WWW under https://doi.org/10.1002/ejic.202100446

heterocyclic plumbylene in catalysis has been presented by Chiu and co-workers.[11]

Besides the coordination chemistry, the tendency of divalent group 14 compounds to participate in insertion and oxidative addition reactions towards main group element-element bonds is well described in the literature.[3i] Several examples for insertion into TM–X bonds are known (TM = transition metal). For instance, Cabeza and García-Álvarez described the reaction between $E[N(SiMe_3)_2]_2$ (E=Ge(II) or Sn(II)) and [AuCl(tht)] (tht = tetrahydrothiophene), which led to the insertion of $E[N(SiMe_3)_2]_2$ into the Au–Cl bond producing **A** and **B** (Scheme 1). They showed as well that PEP pincer 2-germa- and 2-stannabenzimidazol-2-ylidenes undergo insertion reactions with various group 9–11 metal halides (one example (**C**) is shown in Scheme 1).[12]

The NON ligand (NON = 4,5-bis(2,6-diisopropylphenyl-amino)-2,7-di-*tert*-butyl-9,9-dimethylxanthene) has been employed in some actinide, yttrium, and zirconium complexes.[13] In main group chemistry, however, fewer examples are known. For instance, Aldridge and Goicoechea have described recently a highly reactive nucleophilic Al(I) compound stabilized by the NON-backbone (**D** in Scheme 1).[14] We became interested in employing the NON ligand for the synthesis of heavy tetrylenes due to the flexibility and feasible coordination of the oxygen donor to the group 14 element, in particular when compared with other diamido tetrylenes. Effects of the large ring-size were also of interest. We report herein on the synthesis and characterization of the target compounds [(NON)E] (with E=Ge, Sn, Pb), including quantum chemical studies on the σ-donor and π-acceptor capacities. Furthermore, we present initial reactivity studies of the tetrylenes towards selected transition metal precursors such as $[Rh(CO)_2Cl]_2$, $[W(CO)_6]$, and $[Ni(CO)_4]$.

Results and Discussion

Synthesis and characterization of the tetrylenes 3–5

Stepwise deprotonation and metathesis are commonly applied methods for the preparation of tetrylene heterocycles, which we also wanted to exploit for the synthesis of NHTs. Initially, we tried to synthesize the germylene [(NON)Ge] (**3**) and the stannylene [(NON)Sn] (**4**) *via* metalation of the readily available literature-known diamine $[NON]H_2$ (**1**) ($[NON]H_2$ = 4,5-bis(2,6-diisopropyl-phenyl-amino)-2,7-di-*tert*-butyl-9,9-dimethylxanthene) with *n*-BuLi and further reaction with $GeCl_2$·dioxane and $SnCl_2$. NMR spectroscopic analysis showed that **3** and **4** could not be obtained in pure form *via* this route. Therefore, we tried transamination between **1** and $E[N(SiMe_3)_2]_2$ (E=Ge, Sn, Pb). For Ge and Sn, no reaction occurred up to 100 °C in toluene. Only the reaction with $Pb[N(SiMe_3)_2]_2$ led to the desired product [(NON)Pb] (**5**) as a purple crystalline solid in 81% yield (Scheme 2). During our studies it turned out that for a full conversion of the reaction it is essential that 5–10 mol% $LiN(SiMe_3)_2$ are present in the reaction mixture. Although the exact reason for the necessary presence of $LiN(SiMe_3)_2$ remains unknown, it appears reasonable to assume that the reaction of **1** with $LiN(SiMe_3)_2$ gives $[NON]Li_2$, followed by transmetallation to **5** and re-generation of $LiN(SiMe_3)_2$. With pure $Pb[N(SiMe_3)_2]_2$, no reaction occurred even after days at 50 °C (Figure 1, top). By addition of $LiN(SiMe_3)_2$, the reaction mixture turned deep purple within minutes (Figure 1, bottom).

Since the direct transamination between **1** and $E[N(SiMe_3)_2]_2$ (with E=Ge, Sn) failed, **5** was subsequently used as the starting material for the synthesis of **3** and **4** by transmetalation with $SnCl_2$ and $GeCl_2$·dioxane in a mixture of toluene and THF. After recrystallization from toluene, **3** was obtained as yellow crystalline material in 51% yield; **4** as orange crystals in 28% yield. As metathesis of Pb is inconvenient due to sensitivity of **5** towards air and moisture, further trials were carried out with the readily available potassium salt $[NON]K_2$ (**2**), which is prepared within seconds by the reaction of $[NON]H_2$ with

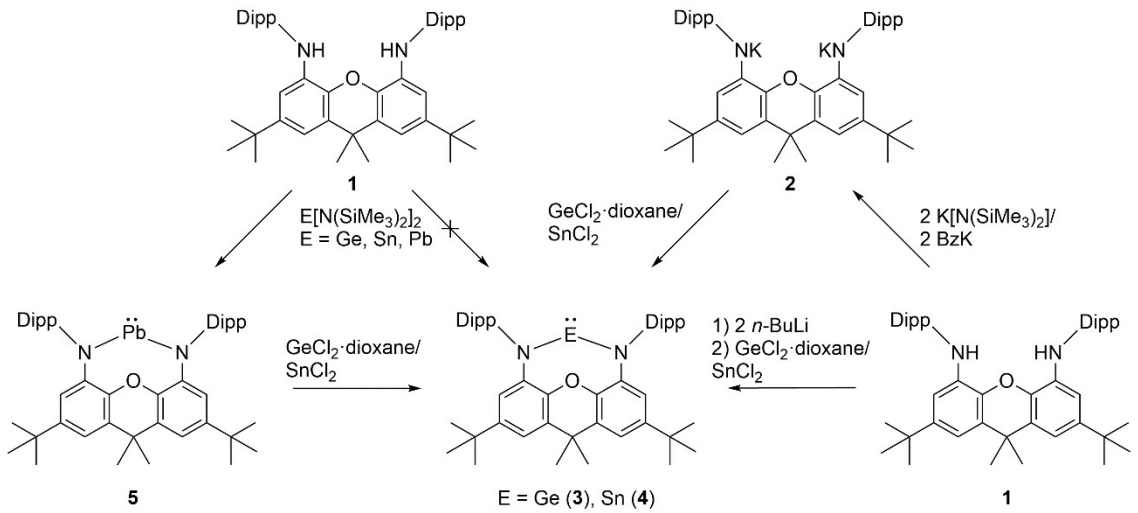

Scheme 2. Reaction scheme for the synthesis of compounds **2**–**5**.

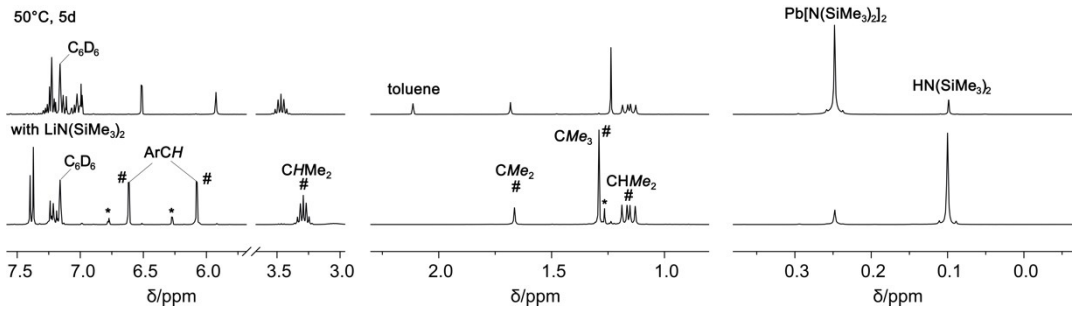

Figure 1. Sections of the ^{1}H NMR spectra of the reaction mixture of [NON]H$_2$ and Pb[N(SiMe$_3$)$_2$]$_2$ at 50 °C (C_6D_6) for 3 days (top) and with addition of LiN(SiMe$_3$)$_2$ (bottom). Signals marked with # belong to [(NON)Pb] (**5**). Signals marked with * belong to [NON]Li$_2$.

benzyl potassium in toluene in an ultrasonication bath (molecular structure in Figure S18, ESI). The reactions between **2** and $SnCl_2$ and $GeCl_2$·dioxane in THF gave **3** and **4** in yields up to 80 %. Crystals suitable for X-ray diffraction were obtained by concentration of toluene solutions of **3** and **4** (Figure 2; space group $P2_1/n$). Crystals of **5** suitable for X-ray analysis were obtained by slow evaporation of a benzene solution (Figure 3; space group $P2_1/n$). All structures contain one co-crystallized solvent molecule, either toluene (**3**, **4**) or benzene (**5**). Due to the sensitivity of **3**–**5** towards air and moisture, no satisfactory elemental analyses were obtained. For the reason that the hydrolysis product **1** has the same solubility and crystallization properties as **3**–**5**, we could just isolate them containing small amounts (ca. 7–10 %, see NMR spectra compiled in the ESI) of the diamine.

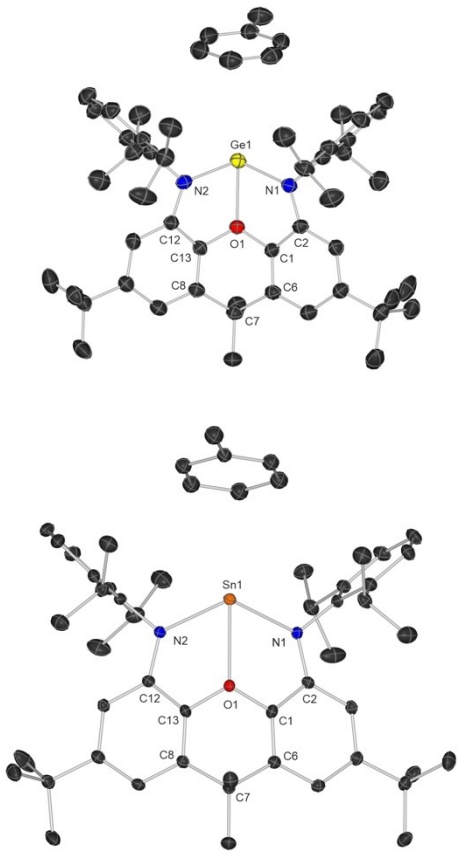

Figure 2. Molecular structures of **3** and **4** (ellipsoids are drawn at the 30 % probability level). Hydrogen atoms are omitted for clarity. Selected bond lengths (Å) and angles (°): **3**: Ge1–N1 = 1.983(3), Ge1–N2 = 1.973(3), Ge1–O1 = 2.213(2); N1–Ge1–O1 = 74.65(10), N2–Ge1–O1 = 75.02(9), N2–Ge1–N1 = 117.6(13), C1–O1–C13 = 110.7(2), C6–C7–C8 = 106.6(3). **4**: Sn1–N1 = Sn1–N2 = 2.182(3), Sn1–O1 = 2.369(2); N1–Sn1–O1 = 70.11(8), N2–Sn1–O1 = 69.59(8), N2–Sn1–N1 = 115.8(10), C1–O1–C13 = 112.6(2), C6–C7–C8 = 107.2(3).

As can be seen from the molecular structures depicted in Fig. 2 and 3, the group 14 atoms are bonded to both nitrogen atoms of the NON framework (N1 and N2). The angles N2–Ge1–N1 = 117.6(12)°, N2–Sn1–N1 = 115.83(10)°, and N2–Pb1–N1 = 113.55(10)° are considerably larger compared to other NHTs composed of five- and six-membered rings (80–90°),[3e,15] ferrocene backbones (100°)[16] and even of acyclic structures (100–105°).[3f]

Due to the coordination of the oxygen atom with a distance of Ge1–O1 = 2.213(2) Å, Sn1–O1 = 2.369(2) Å, and Pb1–O1 = 2.486(2) Å, and the fact that the NON scaffold and the group 14 element atom produce an eight-membered ring structure, a wider angle is expected. Typical N–E–N angles in structurally related [(NON)M(L)$_x$] compounds with M = Th, U, Y, Al(III) and Al(I) fall in the range of ca. 124–135°.[13a–c,14] The NON backbone is folded by 46–42° (Figure 3), which falls in between the Al(I) (~47°)[14] and the Al(III) (~39°) compound;[13c] however, the structures of **3**–**5** are far more bent than the similar thorium and yttrium complexes (~25°).[13a,c] ^{1}H NMR spectroscopic studies revealed, however, that the backbone is rather flexible; only one signal is observed for the two backbone-associated methyl groups in **3** at δ_{1H} = 1.65 ppm, which is indicative for a dynamic "butterfly" interconversion of the NON framework in solution.

Reactivity towards [Rh(CO)$_2$Cl]$_2$

In order to explore the donor properties of the title compounds, we intended to extract TEP values from the corresponding {Rh(CO)$_2$Cl} complexes of **3**–**5**. We therefore treated benzene solutions of **3**–**5** with 1/2 equiv. of the dimer [Rh(CO)$_2$Cl]$_2$. With the germylene (**3**) and plumbylene (**5**), no reaction occurred as

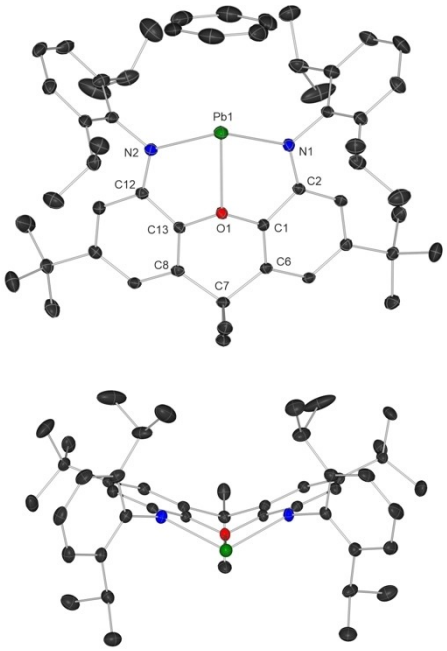

Figure 3. Molecular structure of **5** (ellipsoids are drawn at the 30% probability level). Hydrogen atoms are omitted for clarity. Selected distances (Å) and angles (°): Pb1–N1 = 2.278(3), Pb1–N2 = 2.295(3), Pb1–O1 = 2.486(2); N1–Pb1–O1 = 67.25(9), N2–Pb1–O1 = 66.68(9), N2–Pb1–N1 = 113.55(10), C1–O1–C13 = 113.1(2), C6–C7–C8 = 107.1(3).

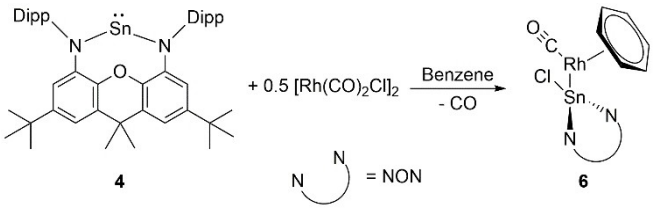

Scheme 3. Synthesis of **6**.

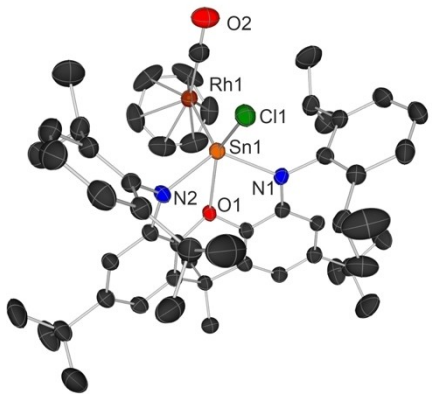

Figure 4. Molecular structure of **6** (ellipsoids are drawn at the 30% probability level). Hydrogen atoms are omitted for clarity. Selected distances (Å) and angles (°): Sn1–N = 2.125(6), Sn1–O1 = 2.338(7), Sn1–Cl1 = 2.383(3), Sn1–Rh1 = 2.5517(11), Cl1–Sn1–Rh1 = 116.61(8), N1–Sn1–N1′ = 122.8(3).

evidenced by ^{1}H NMR spectroscopic monitoring of the reaction. Instead of simply forming an NHT complex of {$Rh(CO)_2Cl$}, the stannylene **4** undergoes an insertion into the Rh–Cl bond (Scheme 3).[17]

By replacing one CO ligand with a η^6-coordinated benzene, the stable complex [(NON)Sn(Cl)Rh(CO)(C_6H_6)] (**6**) is formed. Crystals suitable for X-ray diffraction were obtained by concentrating a benzene solution of **6** (Figure 4; space group $Pmn2_1$).

The Sn1–N = 2.125(6) Å and Sn1–O1 = 2.338(7) Å bonds in **6** are shortened compared to the distances in **4**. In addition, the angle N1–Sn1–N2 = 122.8(3) ° is much more acute as compared to **4**. Due to the poor solubility of the product after crystallization and the slow decomposition in solution, we were unfortunately not able to obtain clean NMR spectra. Nevertheless, the IR spectrum (Figure 5) shows one CO vibration at 2024 cm^{-1}.

In addition to this, three vibrations of the η^6-coordinated benzene at 678 cm^{-1} (C–H deformation), 1978 cm^{-1} and 2089 cm^{-1} (overtone vibrations) are observed. To further support the experimental findings, we carried out DFT calculations at the TPSS/def2-TZVP level of theory. The measured CO vibration is in good agreement with the calculated value of 1993 cm^{-1}.

Reacting one equivalent of the dimer $[Rh(CO)_2Cl]_2$ with **4** also furnished a Rh–Cl insertion product (Scheme 4), although of different composition as evidenced by the IR spectrum (see below).

Suitable single crystals of the complex [(NON)Sn(Cl)$Rh_2(CO)_4Cl$] (**7**) were obtained by slowly concentrating a

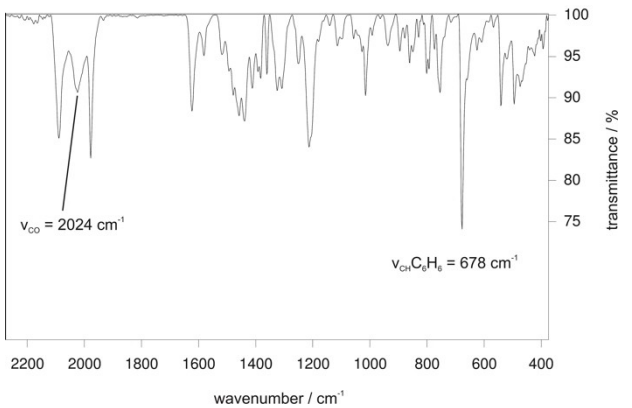

Figure 5. Experimental infrared spectrum of **6** (ATR).

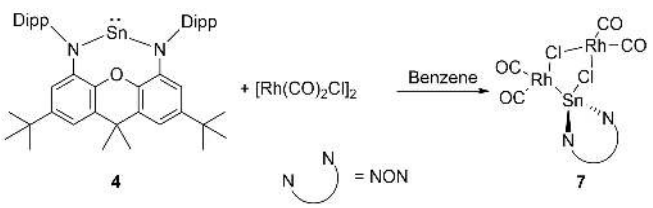

Scheme 4. Synthesis of **7**.

benzene solution of **7** and studied by X-ray diffraction (Figure 6; space group $P2_1/n$).

The molecular structure depicted in Figure 6 reveals a largely intact $[Rh(CO)_2Cl]_2$ dimer in which the stannylene inserted into one Rh–Cl bond. The tin nitrogen bond lengths of 2.115(2) (Sn1–N1) and 2.111(2) Å (Sn1–N2) as well as the distance Sn1–O1 = 2.287(2) Å in **7** are shortened compared to the stannylene **4**. Noteworthy is the slight shortening of the CO bond of the carbonyl ligand *trans* to the tin atom, which is about 2 pm shorter than the other carbonyl bonds. This is in good agreement with the 10 pm elongated Rh1–C55 bond (1.922(4) Å) due to *trans*-influence and thus weakening of the *trans*-Rh–CO bond.[18]

The Sn1–Rh1 bond length of 2.5998(3) Å is ca. 5 pm longer as compared to complex **6**; we also detected a slightly larger N1–Sn1–N2 angle of 118.87(9)°. As expected for the unsymmetrical structure of **7**, NMR studies in solution gave two sets of signals for the isopropyl moieties of the Dipp substituents. Four doublets at δ_{1H} = 1.66; 1.61; 1.39 and 1.12 ppm were detected, which belong to the methyl groups. Also, the C–H protons gave two septets at δ_{1H} = 4.06 and 3.61 ppm, respectively. In contrast to **3**–**5**, the "butterfly" interconversion of the NON framework is hindered in **7**, which is indicated by two signals for the backbone-associated methyl groups showing two distinct signals at δ_{1H} = 1.61 and 1.39 ppm. In the ^{119}Sn NMR spectra, one doublet at δ_{119Sn} = −174.2 ppm with a coupling constant of $^1J_{Sn\text{-}Rh}$ = 802.23 Hz is observed. The IR spectra of **7** (Figure 7) shows four stretching vibrations between 2004–2094 cm^{-1}, which was also supported by DFT calculations at the PBE0[24a]/def2-SVP level of theory.

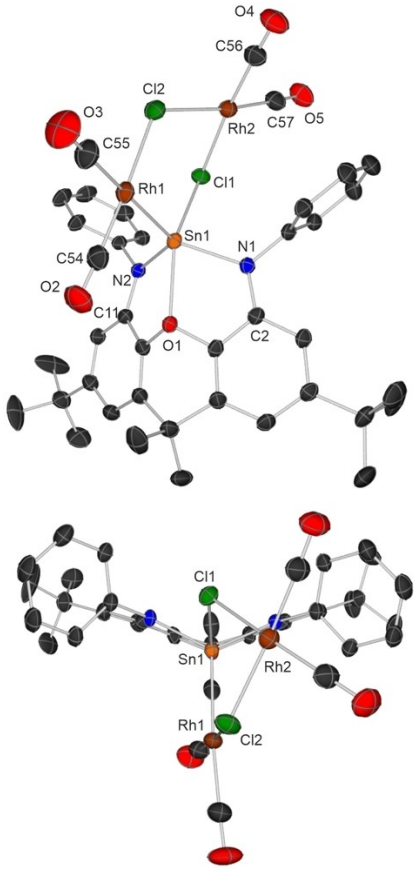

Figure 6. Molecular structure of **7** (ellipsoids are drawn at the 30% probability level). Hydrogen atoms, isopropyl groups and one toluene solvent molecule are omitted for clarity. Selected distances (Å) and angles (°): Sn1–N1 = 2.115(2), Sn1–N2 = 2.111(2), Sn1–O1 = 2.287(2), Sn1–Cl1 = 2.5433(8), Sn1–Rh1 = 2.5998(3), O2–C54 1.144(5), C55–O3 = 1.126(5), O4–C56 = 1.144(4), O5–C57 = 1.140(4), N1–Sn1–N2 = 118.87(9), Rh1–Cl2 = 2.3835(10), Rh2–Cl1 = 2.3727(8), Rh2–Cl2 = 2.3725(9), Rh1–C54 = 1.812(4), Rh1–C55 = 1.922(4), Rh2–C57 = 1.836(4), Rh2–C56 = 1.824(4).

Reactivity of 3–5 towards transition metal carbonyls

Generating $\{W(CO)_5\}$ fragments in situ from $[W(CO)_6]$ by oxidation of one CO with $ONMe_3$, followed by addition of a donor ligand, is a common synthetic route to generate $\{W(CO)_5\}$ complexes (Scheme 5).[19] After adding THF to a mixture of $[W(CO)_6]$ and $ONMe_3$, followed by stirring for one hour at room temperature, the tetrylenes **3**–**5** were added to the respective reaction mixtures.

Additional stirring overnight, evaporation of all volatiles and ^{1}H NMR spectroscopic monitoring revealed, however, that the remaining powders solely contain $[Me_3N{-}W(CO)_5]$ ($\delta_{1H}(NMe_3)$ = 2.00 ppm) and the hydrolysis products of **3**–**5** ($\delta_{1H}(NH)$ = 5.95 ppm). Furthermore, two signals in the ^{13}C NMR spectra at

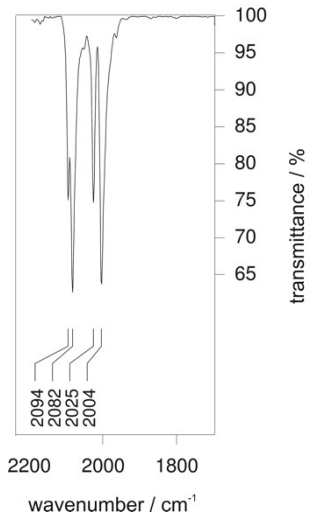

Figure 7. Region of CO vibrations of the IR spectrum of **7**.

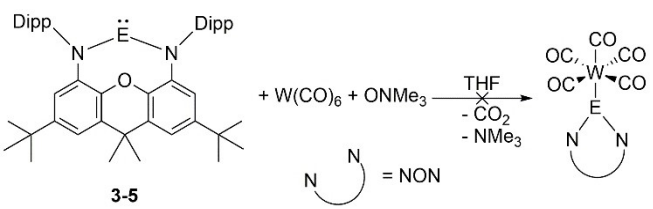

Scheme 5. Anticipated scheme for the synthesis of the [(NON)E–W(CO)5] complexes.

δ_{13C} = 199.6 and 201.3 ppm belonging to the CO carbon atoms, further underline the formation of [Me_3N–$W(CO)_5$] (for details see ESI, Section S1). We believe the inhibited reactivity of the NHTs can at least partly be attributed to steric and kinetic effects.

In order to further probe the coordination properties of the NHTs, **3**–**5** were reacted with [$Ni(CO)_4$] in toluene (Scheme 6).

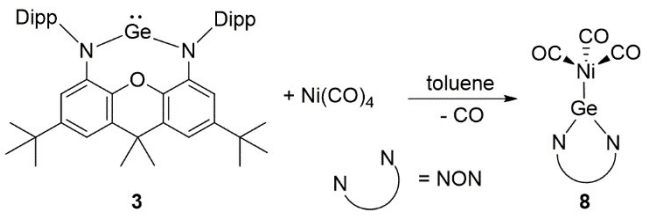

Scheme 6. Synthesis of [(NON)Ge–$Ni(CO)_3$] (**8**).

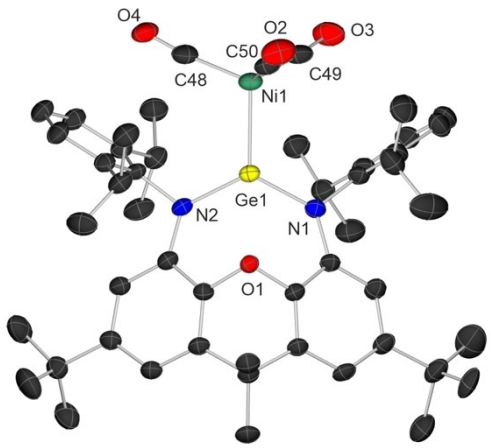

Figure 8. Molecular structures of **8** (ellipsoids are drawn at the 30% probability level). Hydrogen atoms are omitted for clarity. Selected distances (Å) and angles (°): Ge1–N1 = 1.890(3), Ge1–N2 = 1.893(3), Ge1–O1 = 2.4911(2), Ge1–Ni1 = 2.3012(6), O2–C50 = 1.147(5), O3–C49 = 1.142(5), O4–C48 = 1.146(5), N2–Ge1–N1 = 121.27(12).

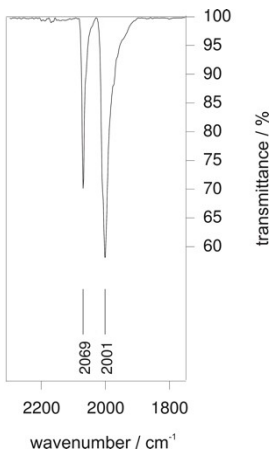

Figure 9. Region of CO vibrations of the IR spectrum of **8**.

Whereas **4** and **5** showed no reactivity, germylene **3** reacted fast with evolution of CO gas after adding [$Ni(CO)_4$], forming the complex [(NON)Ge–$Ni(CO)_3$] (**8**). Crystals suitable for X-ray diffraction were obtained by concentrating a toluene solution of **8** (Figure 8; space group $P\bar{1}$.

The Ge1–O1 distance of 2.4911(2) Å is elongated by 28 pm, accompanied by a 9 pm shortening of the germanium nitrogen bonds of Ge1–N1 = 1.890(3) and Ge1–N2 = 1.893(3) Å, compared to the parent compound **3**. The Ge1–Ni1 bond length of 2.3012(6) falls in the typical range of germylene nickel carbonyl complexes.[20] ^{1}H and ^{13}C NMR spectroscopic studies further confirmed the formation of **8**. ^{13}C NMR spectra of the reaction mixtures in toluene (δ_{13C} = 193.36 ppm for the CO ligands; ESI Figure S3) showed a 2 ppm downfield shifted as compared to [$Ni(CO)_4$] (δ_{13C} = 191.32 ppm). As can be seen from Figure S4 (ESI), the ^{1}H NMR chemical shifts of the iso-propyl moieties, as well as the shifts for the backbone-associated *tert*-butyl and methyl groups and the aromatic protons, changed significantly. The IR spectrum of **8** (Figure 9) shows two bands in the typical carbonyl region, one at 2001 cm^{-1} for the unsymmetrical CO stretch (E, ν_e) and one at 2069 cm^{-1} for the symmetrical CO stretch (A_1, ν_a). The latter can be correlated to the TEP value, which is similar to that of PPh_3 (2069 cm^{-1})[21] and close to the range reported for "typical" *N*-heterocyclic germylenes (2073–2080 cm^{-1}).[22] Nevertheless, lower TEP values have also been reported for germylenes with a [3]ferrocenophane backbone, for instance.[16]

Quantum chemical studies

To further support the experimental findings, DFT[23] calculations were performed on the TPSS[24b]/def2-TZVP[25] level of theory for a series of complexes [(NON)E–$Ni(CO)_3$] (E=Si, Ge, Sn, Pb). As can be seen from Table 1, the calculated vibrational frequencies for [(NON)Ge–$Ni(CO)_3$] are in good agreement with the experimentally observed vibrations of complex **8**. Due to decreasing [(NON)E–$Ni(CO)_3$] bond strengths descending the group 14 coordinating atom, the A_1 CO vibration frequencies ν_a increase (Table 1).

To compare the σ-donor and π-acceptor properties of **3**–**5**, DFT calculations (TPSS/def2-TZVP) were performed (Figure 10). For comparison, the not yet synthesized silylene [(NON)Si)] (**qSi**) was also included in our study. In order to obtain a comprehensive picture, the proton affinities were calculated for determining the donor capacities of the (potential) ligands. Furthermore, we have calculated the rotational barriers of the

Table 1. Calculated average asymmetrical CO vibrations avg ν_e and symmetrical CO vibrations ν_a of [(NON)E–$Ni(CO)_3$] complexes with E=Si, Ge, Sn and Pb in cm^{-1}.

compound	avg ν_e	ν_a
[(NON)Si–$Ni(CO)_3$]	1994.945	2046.08
[(NON)Ge–$Ni(CO)_3$]	2006.545	2057.28
[(NON)Sn–$Ni(CO)_3$]	2014.335	2063.01
[(NON)Pb–$Ni(CO)_3$]	2014.895	2059.86

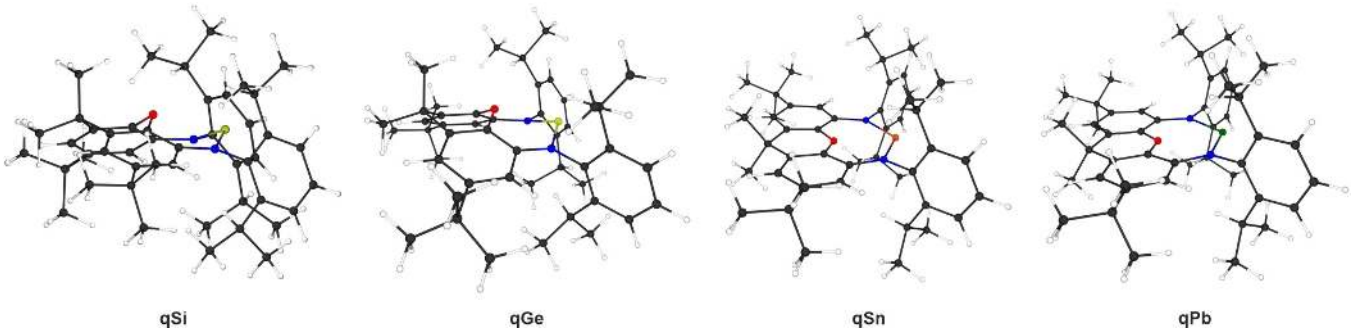

Figure 10. Calculated minimum structures optimized at the TPSS/def2-TZVP level of theory: The sequence silylene **qSi**, germylene **qGe**, stannylene **qSn** and plumbylene **qPb**

E═P bond in the hypothetical structures [NON]E═P-H, relative to H_2E═P-H for determining the acceptor properties.[9] However, due to inconsistencies of the calculated values caused by the σ-proportion to the E═P bond no clear trend was obtained (for more information see ESI page S17). To compare the influence of the NON scaffold towards donor and acceptor capacities, four model systems with different ring-sizes and with or without an oxygen donor were calculated (Scheme 7).

Table 2 shows selected parameters of the optimized structures in comparison to experimental XRD data. The agreement between **3**–**5** and the computed bond length for **qGe**, **qSn** and **qPb** is satisfactory. It has to be noted, however, that the gas-phase calculations of **4** and **5** predict a rather flat backbone with bending angles of only ca. 2°, which is in stark contrast to the molecular structures showing values of ca. 42–46°.

Nevertheless, this finding would be in accordance with the NMR spectroscopic results of the structural flexibility of the scaffold, once coordinated to the divalent group 14 element.

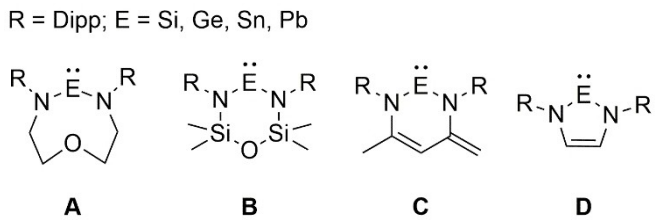

Scheme 7. Calculated model systems: **A**: eight-membered ring with oxygen donor; **B**: six-membered ring with oxygen donor; **C** six-membered ring without oxygen donor; **D** five-membered ring without oxygen donor.

Table 2. Selected geometry parameters (bond length in Å, angles in °) of **3**–**5** and the optimized structures.

compound	E–N/Å	E–O/Å	N–E–N/°	bending/°
3 (XRD)	1.978	2.213	117.6	46
qGe	1.926	2.672	122.8	50.7
4 (XRD)	2.182	2.369	115.8	43
qSn	2.164	2.714	127.7	2.4
5 (XRD)	2.287	2.486	113.6	42
qPb	2.213	2.732	126.8	1.4

The calculated proton affinities span a wide range depending on the identity of both the group 14 element and the backbone. Values between ca. 776 and 1096 kJ/mol have been obtained. The donor capacities decrease upon descending the group 14 element center (Table 3). The compounds **3**–**5** as well as **qSi** are stronger σ-donors than the six-membered ring systems **B** and **C** (and most five-membered ring systems **D** as well) due to their higher proton affinity. We assume that this is an effect of the relatively short E–O distances and the accompanying electron donation to the group 14 element center. In this line of thought, the tetrylenes **3**–**5** show very similar donor capacities as the eight-membered model systems **A**.

For closer investigation of σ and π interactions and their dependence on E, we calculated the complexes [(NON)E–Ni(CO)$_3$] with E═Si, Ge, Sn, Pb, with the E–Ni axis oriented in z direction. As evident from Table 4, the energy for breaking this bond without structure relaxation of the fragments, E_{frag}, is highest for Si and lowest for Pb, whereas Ge and Sn are in-between with similar values. The same holds for the energies after structure relaxation. With the orientation mentioned above, π-acceptance may be quantified by the differences in the population[26] of the p_x(E) and p_y(E) orbitals in [(NON)E–Ni(CO)$_3$] compared to that in the NHTs [(NON)E], Δp_π, σ-donation by corresponding differences for the s(E) and p_z(E) orbitals, Δs and Δp_σ. They are listed in Table 4, together with the resulting π/σ ratio and the sum of the absolute values, as a measure for the total electron density change, $\Sigma|\Delta|$. The sequence for $\Sigma|\Delta|$ follows the sequence of fragmentation or bond energies. The accepting character of p_π(E) systematically decreases from Si to Pb, whereas the numbers for σ-donation

Table 3. Calculated proton affinities of **3**–**5** and the model compounds in kJ/mol.

Backbone	E═Si	E═Ge	E═Sn	E═Pb
NON	1086.83	962.44	902.20	873.10
A	1096.43	961.35	910.67	836.39
B	1017.72	919.60	848.78	776.28
C	964.30	870.51	801.18	819.29
D	927.74	902.38	917.02	927.83

Table 4. [(NON)E–Ni(CO)$_3$], E=Si, Ge, Sn, Pb. E_{frag} (in kJ/mol) is the energy needed for the fragmentation to [(NON)E] and {Ni(CO)$_3$}, without structure relaxation of the fragments, E_{bond} that with relaxation. E_{rot} is the rotation barrier, $E_{rot,\ without\ Ni}$ is the difference of single point energies with Ni removed from both the rotational transition state and the minimum structure. Δs, Δp_σ and Δp_π are the differences of Mulliken populations at the E atom between the entire molecule and the (non-relaxed) fragment [(NON)E] for the s functions (Δs), the p-functions along the E–Ni axis (Δp_σ), and the sum of the p-functions perpendicular to the axis (Δp_π).

	E=Si	E=Ge	E=Sn	E=Pb
E_{frag}	173.3	118.4	94.4	56.2
E_{bond}	118.4	65.0	63.6	33.0
E_{rot}	75.6	8.3	34.3	38.8
$E_{rot,\ without\ Ni}$	42.9	−2.2	16.6	20.0
Δs	0.272	0.318	0.240	0.127
Δp_σ	0.263	0.051	0.085	0.012
Δp_π	−0.215	−0.187	−0.132	−0.045
$\Sigma\lvert\Delta\rvert = \Delta s + \Delta p_\sigma - \Delta p_\pi$	0.750	0.556	0.457	0.184
$\pi/\sigma = -\Delta p_\pi/(\Delta s + \Delta p_\sigma)$	0.401	0.507	0.406	0.324

are less systematic. Donation from s(E) is by far smallest for Pb, because of its comparably low energy due to scalar relativistic effects, but also donation from its p_σ orbital is very small. Overall, the π/σ ratios range from 0.32 and 0.51, which is significantly less than e.g. for a C atom in [Ni(CO)$_4$], where π/σ amounts to 0.98 (calculated with the same method). On the other hand, the total electron density changes, $\Sigma|\Delta|$, for E=Si (or Ge) are similar to that for a C atom in [Ni(CO)$_4$], 0.602, and same holds for the bond energy of the fourth CO in [Ni(CO)$_4$] 122.4 kJ/mol. The strengths of the π interactions are not well correlated to the height of the rotational barriers. The latter were estimated with a nudged-band type optimization tool.[27] The highest barrier, 75.6 kJ/mol, is observed for E=Si, the lowest for E=Ge (8.3 kJ/mol)), the barriers for the Sn and Pb ligands are in-between. Obviously, there are other effects like the interactions of CO with H atoms of Dipp that are at least as important for the barrier height. In fact, when removing the source of π interactions, that is, removing the Ni atom from both the minimum and the rotational transition state for each compound, the differences of the single point energies for transition and ground state reveal a very similar pattern as with Ni. The largest difference is found for E=Si (42.9 kJ/mol), the lowest for E=Ge (−2.2 kJ/mol), and Sn and Pb are in-between again.

Conclusion

In this work, we report different pathways for the synthesis of *N*-heterocyclic tetrylenes stabilized by the NON-donor ligand 4,5-bis(2,6-diisopropylphenyl-amino)-2,7-di-*tert*-butyl-9,9-dimethyl-xanthene. The title compounds **3**–**5** have been fully characterized and their molecular structures were determined by X-ray diffraction. Quantum chemical studies on the σ-donor and π-acceptor capacities revealed that **3**–**5** feature high donor and acceptor strengths compared to related model systems. Furthermore, the reactivity towards transition metal carbonyls [Rh(CO)$_2$Cl]$_2$, [W(CO)$_6$] and [Ni(CO)$_4$] were investigated. Complex **6** and **7** showing the diverse reactivity of NHTs compared to NHCs. Instead of simply coordinating to the {Rh(CO)$_2$Cl} fragment, **4** undergoes insertion into the Rh–Cl bond. When insertion reactions are prevented by avoiding halogenated transition metal precursors, germylene **3** shows "classical" coordination chemistry by forming the {Ni(CO)$_3$} complex **8**. The exemplary investigation of [(NON)E–Ni(CO)$_3$] showed that the bond strength of this ligand for E=Si is similar to that of CO, for E=Ge or Sn it is about half of that of CO, and for Pb about a quarter of that of CO. Similar trends hold for the changes of the sum of absolute numbers of occupations of σ- and π-type orbitals when {Ni(CO)$_3$} approaches CO or [(NON)E]. In contrast, the ratio of changes in occupations σ- and π-type orbitals is different: Whereas for CO, they are almost identical ($\pi/\sigma \approx 1$), for [(NON)E] this ratio amounts to 1/2 or less, depending on the choice of E. Studies in our lab continue to further explore the coordination chemistry and general reactivities of the NON-ligated and related tetrylens.

Experimental Section

General methods. All operations were carried out under dry argon using standard Schlenk and glovebox techniques. [NON]H$_2$[13a], E[N(SiMe$_3$)$_2$]$_2$[28] where synthesized according to literature procedures. Solvents where dried over Na/K and rigorously degassed before use. NMR spectra where recorded on Bruker AV 300 and 400 spectrometers in dry degassed deuterated solvents. ^{1}H and ^{13}C{^{1}H} chemical shifts where reported against TMS. ^{119}Sn and ^{207}Pb chemical shifts with respect to SnMe$_4$ and PbMe$_4$. Coupling constants (*J*) are given in Hertz as positive values, regardless of their real individual signs. The multiplicity of the signals is indicated as s, d, q, sept, or m for singlet, doublet, quartet, septet, or multiplet, respectively. The assignments were confirmed, as necessary, with the use of 2D NMR correlation experiments. IR spectra were measured with a Bruker Alpha spectrometer by using the attenuated total reflection (ATR) technique on powdered samples, and the data are quoted in wavenumbers (cm^{-1}). The intensity of the absorption band is indicated as vw (very weak), w (weak), m (medium), s (strong), vs (very strong), and br (broad). Elemental analyses were carried out in the institutional technical laboratories of the Karlsruhe Institute of Technology (KIT). Due to extremely high sensitivity towards air and moisture no satisfactory elemental analysis were obtained for **3**–**8**.

Safety Precautions in Handling with [Ni(CO)$_4$]: Special care has been taken while manipulating the extremely toxic, flammable and volatile (b.p. 43 °C) [Ni(CO)$_4$]. All manipulations were carried out in a well-ventilated hood or a glovebox. Safety glasses, an apron and gloves using additional protective gloves should be worn when handling this reagent. [Ni(CO)$_4$] should be maintained at temperatures below 0 °C. Traces of [Ni(CO)$_4$] can be disposed by treatment with half-concentrated nitric acid and all glassware used should be treated with half concentrated nitric acid.

[NON]K$_2$·toluene (2). A Schlenk flask was charged with [NON]H$_2$ (1.5 g, 2.23 mmol) and BzK (0.595 g, 4.57 mmol) in toluene (18 ml). After five minutes in an ultrasonic bath, filtration, removing of the volatiles and drying under high vacuum **2** was isolated as colorless powder (1.6 g, 1.9 mmol, 80 %). Crystals suitable for XRD were obtained by concentration and cooling a solution in toluene to 4 °C. ^{1}H NMR (300 MHz, C$_6$D$_6$): δ 7.30–7.18 (m, 6H, Ar-*H*), 6.59 (d, 2H, ^4J 2.19 Hz, C*H*^{3}), 6.19 (d, 2H, ^4J 2.05 Hz, C*H*^{1}), 2.91 (sept, 4H, ^3J 7.02 Hz, C*H*Me$_2$), 1.85 (s, 6H, C*Me$_2$*), 1.40 (s, 18H, C*Me$_3$*), 1.24 (d, 12H, ^3J 6.75 Hz, CH*Me$_2$*), 1.00 (d, 12H, ^3J 7.15 Hz, CH*Me$_2$*).

[(NON)Ge]·toluene (3·toluene). Via transmetalation: A Schlenk flask was charged with **1** (70 mg, 72 μmol), $GeCl_2$·dioxane (20 mg, 86 μmol) and toluene (5 ml). After addition of THF (1 ml), the color changed immediately to yellow. After stirring over night, the reaction mixture was filtrated and concentrated. Cooling to 4 °C, removal of the supernatant and drying in high vacuum yielded **3** (30.7 mg, 37 μmol, 51 %) as yellow crystalline solid.

Via salt metathesis: In an argon filled glovebox a vial was charged with **2** (0.5 g, 0.59 mmol) and THF (8 ml). After addition of a solution of $GeCl_2$·dioxane (127 mg, 0.59 mmol) in THF (2 ml), the color changed from slightly green to yellow and the mixture becomes cloudy. Filtration, evaporation of all volatiles and drying under high vacuum yielding **3·THF** (350 mg, 0.47 mmol, 80 %) as a yellow powder. Crystals suitable for XRD were obtained by concentration a solution in toluene. ^{1}H NMR (300 MHz, C_6D_6): δ 7.27 (s, 6H, Ar-*H*), 6.84 (d, 2H, ^4J 1.9 Hz, C*H*^{3}), 6.37 (d, 2H, ^4J 1.9 Hz, C*H*^{1}), 3.51 (sept, 4H, ^3J 6.79 Hz, C*H*Me$_2$), 1.65 (s, 6H, C*Me$_2$*), 1.22 (d, 12H, ^3J 6.98 Hz, CH*Me$_2$*), 1.19 (s, 18H, C*Me$_3$*), 1.13 (d, 12H, ^3J 6.78 Hz, CH*Me$_2$*). ^{13}C{^{1}H} NMR (75 MHz, C_6D_6): δ 149.1 (Ar-C_{ipso}), 148.6, 145.1, 140.6 (Xanth-*Q*), 137.8 (Ar-C_{ortho}), 135.8 (Ar-CH_{para}), 124.6 (Ar-CH_{meta}), 110.8 (*C*H^3), 109.81 (*C*H^1), 38.6 (*C*Me$_2$), 35.2 (*C*Me$_3$), 31.8 (C*Me$_2$*), 29.0 (C*Me$_3$*), 27.0 (*C*HMe$_2$), 25.5, 24.4 (CH*Me$_2$*).

[(NON)Sn]·toluene (4·toluene). Via transmetalation: A Schlenk flask was charged with **1** (70 mg, 72 μmol), $SnCl_2$ (16.4 mg, 86 μmol) and toluene (5 ml). After addition of THF (1 ml), the color changed immediately to deep orange. After stirring over night, the reaction mixture was filtrated and concentrated. Cooling to 4 °C, removal of the supernatant and drying in high vacuum yielded **4** (17.5 mg, 20 μmol, 28 %) as orange crystalline solid.

Via salt metathesis: In an argon filled glovebox a vial is charged with **2** (1.0 g, 1.19 mmol) and THF (10 ml). After addition of a solution of $SnCl_2$ (225 mg, 1.19 mmol) in THF (5 ml), the color changed from slightly green to orange and the mixture became cloudy. Filtration, evaporation of all volatiles and drying under high vacuum yielded **4·THF** (820 mg, 0.95 mmol, 80 %) as an orange powder. Crystals suitable for XRD were obtained by concentration and cooling a solution in toluene to 4 °C. ^{1}H NMR (300 MHz, C_6D_6): δ 7.29 (m, 6H, Ar-*H*), 6.81 (d, 2H, ^4J 2.02 Hz, C*H*^{3}), 6.33 (d, 2H, ^4J 2.0 Hz, C*H*^{1}), 3.41 (sept, 4H, ^3J 6.87 Hz, C*H*Me$_2$), 1.61 (s, 6H, C*Me$_2$*), 1.25 (s, 18H, C*Me$_3$*), 1.19 (d, 12H, ^3J 6.92 Hz, CH*Me$_2$*), 1.15 (d, 12H, ^3J 6.64 Hz, CH*Me$_2$*). ^{13}C{^{1}H} NMR (75 MHz, C_6D_6): δ 148.0 (Ar-C_{ipso}), 143.0, 141.5, 139.4 (Xanth-*Q*), 132.9 (Ar-C_{ortho}), 126.9 (Ar-CH_{para}), 124.3 (Ar-CH_{meta}), 109.5 (*C*H^3), 107.8 (*C*H^1), 36.9 (*C*Me$_2$), 35.1 (*C*Me$_3$), 31.9 (C*Me$_2$*), 28.8 (C*Me$_3$*), 28.6 (*C*HMe$_2$), 25.9, 25.6 (CH*Me$_2$*). ^{119}Sn NMR (112 MHz, C_6D_6): δ 55.7 ppm.

[(NON)Pb]·toluene (5·toluene). A Schlenk flask was charged with [NON]H_2 (2 g, 2.97 mmol), Pb[N(SiMe_3)$_2$]$_2$ (1.726 g, 3.27 mmol) and toluene (40 ml). The reaction mixture became deep purple within 30 minutes. After stirring for 16 hours, a deep purple crystalline solid formed. Filtration *via* cannula and drying under high vacuum yielded (2.33 g, 2.4 mmol, 81 %) **5**. Crystals suitable for XRD were obtained by slow solvent evaporation from benzene. ^{1}H NMR (300 MHz, C_6D_6): δ 7.38 (m, 4H, Ar-*H*), 7.22 (m, 2H, Ar-*H*), 6.62 (d, 2H, ^4J 2.11 Hz, C*H*^{3}), 6.08 (d, 2H, ^4J 2.08 Hz, C*H*^{1}), 3.29 (sept, 4H, ^3J 6.87 Hz, C*H*Me$_2$), 1.66 (s, 6H, C*Me$_2$*), 1.29 (s, 18H, C*Me$_3$*), 1.18 (d, 12H, ^3J 6.83 Hz, CH*Me$_2$*), 1.14 (d, 12H, ^3J 6.93 Hz, CH*Me$_2$*). ^{13}C{^{1}H} NMR (75 MHz, C_6D_6): δ 146.2 (Ar-C_{ipso}), 145.1, 144.9, 141.4 (Xanth-*Q*), 130.6 (Ar-C_{ortho}), 126.5 (Ar-CH_{para}), 123.9 (Ar-CH_{meta}), 111.3 (*C*H^3), 108.1 (*C*H^1), 36.1 (*C*Me$_2$), 35.2 (*C*Me$_3$), 32.0 (C*Me$_2$*), 30.8 (C*Me$_3$*), 37.5 (*C*HMe$_2$), 26.4, 25.9 (CH*Me$_2$*). ^{207}Pb NMR (63 MHz, C_6D_6): δ 2927.9 ppm.

[(NON)Sn(Cl)Rh(CO)(C_6H_6)] (6). A Schlenk flask was charged with **4·toluene** (50 mg, 56 μmol), $[Rh(CO)_2Cl]_2$ (11 mg, 28 μmol) and benzene (5 ml). While stirring for 2 days, the solution becomes dark red. Concentration of the solution to incipient crystallization and keeping it at ambient temperature gave 14 mg (14 μmol, 25 %) of **6** in form of dark red crystals. (Because of the poor solubility of the product after crystallization and the slow decomposition in solution, we could not obtain clean NMR spectra.)

[(NON)Sn(Cl)Rh_2(CO)$_4$(Cl)] (7). A Schlenk flask was charged with **4·toluene** (100 mg, 0.12 mmol), $[Rh(CO)_2Cl]_2$ (45 mg, 0.12 mmol) and a mixture of toluene/THF (2 : 1, 15 ml). While stirring for 1 hour, the solution became dark red. Filtration and slow solvent evaporation yielded 104 mg (0.08 mmol, 68 %) of **7** in form of dark red crystals. ^{1}H NMR (300 MHz, C_6D_6): δ 7.25 (m, 6H, Ar-*H*), 6.76 (d, 2H, ^4J 1.97 Hz, C*H*^{3}), 6.25 (d, 2H, ^4J 1.97 Hz, C*H*^{1}), 4.06 (sept, 2H, ^3J 6.72 Hz, C*H*Me$_2$), 3.61 (sept, 2H, ^3J 6.72 Hz, C*H*Me$_2$), 1.68 (d, 6H, ^3J 4.42 Hz, CH*Me$_2$*), 1.64 (d, 6H, ^3J 6.95 Hz, CH*Me$_2$*) 1.61 (s, 3H, C*Me$_2$*), 1.39 (s, 3H, C*Me$_2$* overlaid with d of CH*Me$_2$*), 1.25 (s, 18H, C*Me$_3$*), 1.39 (d, 6H, ^3J 6.93 Hz, CH*Me$_2$*), 1.12 (d, 6H, ^3J 6.54 Hz, CH*Me$_2$*). ^{13}C{^{1}H} NMR (75 MHz, C_6D_6): δ 149.6, 148.8, 148.1, 147.8, 146.1, 141.3, 140.0, 136.4, 136.2, 135.9, 135.1, 111.8, 108.2 (Ar–C) 38.0 (*C*Me$_2$), 35.2 (*C*Me$_3$), 31.7 (C*Me$_2$*), 29.0 (C*Me$_3$*), 29.0, 28.7 (*C*HMe$_2$), 26.7, 26.4, 26.1, 24.7 (CH*Me$_2$*). ^{119}Sn NMR (112 MHz, C_6D_6): δ −174.2 (d, *J* 802.23 Hz) ppm.

[(NON)Ge-Ni(CO)$_3$] (8). To a Schlenk flask with **3·toluene** (50 mg, 60 μmol) and 3 ml toluene a 0.16 M solution of [Ni(CO)$_4$] (0.46 ml, 73 μmol) was added at room temperature. The yellow reaction mixture became pale yellow and the evolution of gas was observed. After stirring for one hour, all volatiles were removed *in vacuo*. **8** was isolated as a greenish yellow powder (48 mg, 54 μmol, 90 %). Crystals suitable for XRD were obtained by slow solvent evaporation from toluene. ^{1}H NMR (300 MHz, C_6D_6): δ 7.24 (m, 6H, Ar-*H*), 6.87 (d, 2H, ^4J 1.93 Hz, C*H*^{3}), 6.23 (d, 2H, ^4J 1.93 Hz, C*H*^{1}), 3.5 (sept, 4H, ^3J 6.45 Hz, C*H*Me$_2$), 1.68 (s, 6H, C*Me$_2$*), 1.34 (d, 12H, ^3J 7.07 Hz, CH*Me$_2$*), 1.09 (s, 18H, C*Me$_3$*), 1.03 (d, 12H, ^3J 7.07 Hz, CH*Me$_2$*). ^{13}C{^{1}H} NMR (75 MHz, C_6D_6): δ 194.4 (*C*O) 149.1, 147.9, 145.9, 141.2, 138.4, 138.2, 114.0, 111.1 (Ar-*C*), 39.3 (*C*Me$_2$), 35.0 (*C*Me$_3$), 31.6 (C*Me$_2$*), 29.2 (C*Me$_3$*), 25.6 (*C*HMe$_2$), 24.8 (CH*Me$_2$*).

Crystallographic details

All the structures have been deposited at the Cambridge Crystallographic Data Centre. CCDC: 2084915 (**2**), 2084916 (**3**), 2084918 (**4**), 2084917 (**5**), 2094670 (**6**), 2094671 (**7**), 2094672 (**8**). For further crystallographic details, see the Supporting Information, Section 3.

Acknowledgements

This work was partly carried out with the support of the Karlsruhe Nano Micro Facility (KNMF), a Helmholtz Research Infrastructure at *Karlsruhe Institute of Technology (KIT)* and we thank Prof. Dieter Fenske and Dr. Alexander Hinz for help with XRD. We thank Dr. Kevin Reiter for help with quantum chemical calculation. Finally, we thank Bernhard Birenheide for the support by solving crystal structures. U. R. and M. S. L. thanks the Julius-Maximilians-Universität Würzburg for support. Open access funding enabled and organized by Projekt DEAL.

Conflict of Interest

The authors declare no conflict of interest.

Keywords: Germylenes · *N*-heterocyclic tetrylenes · *N*-hetrocyclic tetrylene complexes · Plumbylenes · Stannylenes

[1] a) A. J. Arduengo, *Acc. Chem. Res.* **1999**, *32*, 913–921; b) W. A. Herrmann, *Angew. Chem. Int. Ed. Engl.* **2002**, *41*, 1290–1309; c) E. Peris, R. H. Crabtree, *Coord. Chem. Rev.* **2004**, *248*, 2239–2246; d) J. A. Mata, M. Poyatos, E. Peris, *Coord. Chem. Rev.* **2007**, *251*, 841–859; e) F. E. Hahn, M. C. Jahnke, *Angew. Chem. Int. Ed. Engl.* **2008**, *47*, 3122–3172; f) S. Díez-González, N. Marion, S. P. Nolan, *Chem. Rev.* **2009**, *109*, 3612–3676; g) O. Schuster, L. Yang, H. G. Raubenheimer, M. Albrecht, *Chem. Rev.* **2009**, *109*, 3445–3478; h) L. Mercs, M. Albrecht, *Chem. Soc. Rev.* **2010**, *39*, 1903–1912; i) M. N. Hopkinson, C. Richter, M. Schedler, F. Glorius, *Nature* **2014**, *510*, 485–496.

[2] a) M. Elie, F. Sguerra, F. Di Meo, M. D. Weber, R. Marion, A. Grimault, J.-F. Lohier, A. Stallivieri, A. Brosseau, R. B. Pansu, J.-L. Renaud, M. Linares, M. Hamel, R. D. Costa, S. Gaillard, *ACS Appl. Mater. Interfaces* **2016**, *8*, 14678–14691; b) D. Janssen-Müller, C. Schlepphorst, F. Glorius, *Chem. Soc. Rev.* **2017**, *46*, 4845–4854; c) H. Wang, G. Lu, G. J. Sormunen, H. A. Malik, P. Liu, J. Montgomery, *J. Am. Chem. Soc.* **2017**, *139*, 9317–9324.

[3] a) A. Meller, C.-P. Gräbe, *Chem. Ber.* **1985**, *118*, 2020–2029; b) W. P. Neumann, *Chem. Rev.* **1991**, *91*, 311–334; c) M. Denk, R. Lennon, R. Hayashi, R. West, A. V. Belyakov, H. P. Verne, A. Haaland, M. Wagner, N. Metzler, *J. Am. Chem. Soc.* **1994**, *116*, 2691–2692; d) T. Gans-Eichler, D. Gudat, M. Nieger, *Angew. Chem. Int. Ed. Engl.* **2002**, *41*, 1888–1891; e) J. P. Charmant, M. F. Haddow, F. E. Hahn, D. Heitmann, R. Frohlich, S. M. Mansell, C. A. Russell, D. F. Wass, *Dalton Trans.* **2008**, 6055–6059; f) Y. Mizuhata, T. Sasamori, N. Tokitoh, *Chem. Rev.* **2009**, *109*, 3479–3511; g) M. Asay, C. Jones, M. Driess, *Chem. Rev.* **2011**, *111*, 354–396; h) S. Krupski, R. Pöttgen, I. Schellenberg, F. E. Hahn, *Dalton Trans.* **2014**, *43*, 173–181; i) T. Chu, G. I. Nikonov, *Chem. Rev.* **2018**, *118*, 3608–3680; M. J. Krahfuss, U. Radius, *Dalton Trans.* **2021**, *50*, 6752–6765.

[4] a) C. Boehme, G. Frenking, *J. Am. Chem. Soc.* **1996**, *118*, 2039–2046; b) O. Kühl, K. Lifson, W. Langel, *Eur. J. Org. Chem.* **2006**, *2006*, 2336–2343.

[5] a) .F. Ullah, G. Bajor, T. Veszpremi, P. G. Jones, J. W. Heinicke, *Angew. Chem. Int. Ed. Engl.* **2007**, *46*, 2697–2700; b) A. V. Zabula, F. E. Hahn, T. Pape, A. Hepp, *Organometallics* **2007**, *26*, 1972–1980.

[6] a) C. Boehme, G. Frenking, *Organometallics* **1998**, *17*, 5801–5809; b) T. A. N. Nguyen, G. Frenking, *Chem. Eur. J.* **2012**, *18*, 12733–12748.

[7] a) M. F. Lappert, R. S. Rowe, *Coord. Chem. Rev.* **1990**, *100*, 267–292; b) D. Heitmann, T. Pape, A. Hepp, C. Mück-Lichtenfeld, S. Grimme, F. E. Hahn, *J. Am. Chem. Soc.* **2011**, *133*, 11118–11120; c) H. Arp, J. Baumgartner, C. Marschner, P. Zark, T. Müller, *J. Am. Chem. Soc.* **2012**, *134*, 10864–10875; d) H. Braunschweig, A. Damme, R. D. Dewhurst, F. Hupp, J. O. C. Jimenez-Halla, K. Radacki, *Chem. Commun.* **2012**, *48*, 10410–10412; e) J. Hlina, H. Arp, M. Walewska, U. Flörke, K. Zangger, C. Marschner, J. Baumgartner, *Organometallics* **2014**, *33*, 7069–7077; f) L. Álvarez-Rodríguez, J. A. Cabeza, P. García-Álvarez, E. Pérez-Carreño, D. Polo, *Inorg. Chem.* **2015**, *54*, 2983–2994; g) L. Álvarez-Rodríguez, J. A. Cabeza, P. García-Álvarez, D. Polo, *Coord. Chem. Rev.* **2015**, *300*, 1–28; h) R. Tacke, T. Ribbeck, *Dalton Trans.* **2017**, *46*, 13628–13659; i) Y.-P. Zhou, M. Driess, *Angew. Chem. Int. Ed. Engl.* **2019**, *58*, 3715–3728; j) G. Bačić, D. Zanders, B. Mallick, A. Devi, S. T. Barry, *Inorg. Chem.* **2018**, *57*, 8218–8226; k) M. Veith, *Angew. Chem. Int. Ed. Engl.* **1975**, *14*, 263–264; l) M. Veith, M. Grosser, *Z. Naturforsch. B* **1982**, *37*, 1375–1381; m) M. Veith, M. Grosser, V. Huch, *Z. Anorg. Allg. Chem.* **1984**, *513*, 89–102; n) S. M. I. Al-Rafia, P. A. Lummis, M. J. Ferguson, R. McDonald, E. Rivard, *Inorg. Chem.* **2010**, *49*, 9709–9717; o) S. K. Liew, S. M. I. Al-Rafia, J. T. Goettel, P. A. Lummis, S. M. McDonald, L. J. Miedema, M. J. Ferguson, R. McDonald, E. Rivard, *Inorg. Chem.* **2012**, *51*, 5471–5480.

[8] a) B. Blom, D. Gallego, M. Driess, *Inorg. Chem. Front.* **2014**, *1*, 134–148; b) Y. Wu, C. Shan, Y. Sun, P. Chen, J. Ying, J. Zhu, L. L. Liu, Y. Zhao, *Chem. Commun.* **2016**, *52*, 13799–13802; c) S. Raoufmoghaddam, Y.-P. Zhou, Y. Wang, M. Driess, *J. Organomet. Chem.* **2017**, *829*, 2–10.

[9] a) Z. Benedek, T. Szilvási, *RSC Adv.* **2015**, *5*, 5077–5086; b) Z. Benedek, T. Szilvási, *Organometallics* **2017**, *36*, 1591–1600.

[10] a) R. Dasgupta, S. Das, S. Hiwase, S. K. Pati, S. Khan, *Organometallics* **2019**, *38*, 1429–1435; b) T. J. Hadlington, M. Hermann, G. Frenking, C. Jones, *J. Am. Chem. Soc.* **2014**, *136*, 3028–3031; c) T. J. Hadlington, M. Driess, C. Jones, *Chem. Soc. Rev.* **2018**, *47*, 4176–4197.

[11] T.-H. Lin, G.-H. Lee, S.-M. Peng, C.-W. Chiu, H.-Y. Chen, *Polymer* **2019**, *180*.

[12] J. A. Cabeza, P. García-Álvarez, C. J. Laglera-Gándara, *Eur. J. Inorg. Chem.* **2020**, *2020*, 784–795.

[13] a) C. A. Cruz, D. J. H. Emslie, L. E. Harrington, J. F. Britten, C. M. Robertson, *Organometallics* **2007**, *26*, 692–701; b) A. Dauth, J. A. Love, *Dalton Trans.* **2012**, *41*, 7782–7791; c) K. S. A. Motolko, D. J. H. Emslie, H. A. Jenkins, *Organometallics* **2017**, *36*, 1601–1608; d) K. S. A. Motolko, J. S. Price, D. J. H. Emslie, H. A. Jenkins, J. F. Britten, *Organometallics* **2017**, *36*, 3084–3093.

[14] J. Hicks, P. Vasko, J. M. Goicoechea, S. Aldridge, *Nature* **2018**, *557*, 92–95.

[15] a) O. Kühl, *Coord. Chem. Rev.* **2004**, *248*, 411–427; b) E. M. B. Moos, W. Feuerstein, F. Krämer, F. Breher, *Z. Anorg. Allg. Chem.* **2018**, *644*, 1115–1122.

[16] a) R. Guthardt, J. Oetzel, J. I. Schweizer, C. Bruhn, R. Langer, M. Maurer, J. Vicha, P. Shestakova, M. C. Holthausen, U. Siemeling, *Angew. Chem. Int. Ed. Engl.* **2019**, *58*, 1387–1391; b) F. Walz, E. Moos, D. Garnier, R. Köppe, C. E. Anson, F. Breher, *Chem. Eur. J.* **2017**, *23*, 1173–1186.

[17] For recent investigations on the insertion of *N*-heterocyclic silylenes into MX or CF bonds, see: a) M. J. Krahfuss, J. Nitsch, F. M. Bickelhaupt, T. B. Marder, U. Radius, *Chem. Eur. J.* **2020**, *26*, 11276–11292; b) M. J. Krahfuss, U. Radius, *Inorg. Chem.* **2020**, *59*, 10976–10985; c) M. W. Kuntze-Fechner, H. Verplancke, L. Tendera, M. Diefenbach, I. Krummenacher, H. Braunschweig, T. B. Marder, M. C. Holthausen, U. Radius, *Chem. Sci.* **2020**, *11*, 11009–11023.

[18] a) A. Pidcock, R. E. Richards, L. M. Venanzi, *J. Chem. Soc. A* **1966**, 1707–1710; b) B. J. Coe, S. J. Glenwright, *Coord. Chem. Rev.* **2000**, *203*, 5–80.

[19] a) C.-C. Yang, W.-Y. Yeh, G.-H. Lee, S.-M. Peng, *J. Organomet. Chem.* **2000**, *598*, 353–358; b) A. K. Adhikari, T. Grell, P. Lönnecke, E. Hey-Hawkins, *Inorg. Chem.* **2018**, *57*, 3297–3304.

[20] a) W. A. Herrmann, M. Denk, J. Behm, W. Scherer, F.-R. Klingan, H. Bock, B. Solouki, M. Wagner, *Angew. Chem. Int. Ed. Engl.* **1992**, *31*, 1485–1488; b) C. Gendy, A. Mansikkamäki, J. Valjus, J. Heidebrecht, P. C.-Y. Hui, G. M. Bernard, H. M. Tuononen, R. E. Wasylishen, V. K. Michaelis, R. Roesler, *Angew. Chem. Int. Ed. Engl.* **2019**, *58*, 154–158; c) P. M. Keil, T. Szilvási, T. J. Hadlington, *Chem. Sci.* **2021**, *12*, 5582–5590.

[21] C. A. Tolman, *Chem. Rev.* **1977**, *77*, 313–348.

[22] Germylenes are usually categorized among the weak σ-donor and good π-acceptor ligands. F. Ullah, O. Kühl, G. Bajor, T. Veszprémi, P. G. Jones, J. Heinicke, *Eur. J. Inorg. Chem.* **2009**, 221–229.

[23] a) TURBOMOLE V7.5.1 2021, a development of University of Karlsruhe and Forschungszentrum Karlsruhe GmbH, 1989–2007, TURBOMOLE GmbH, since 2007; available from http://www.turbomole.com; b) F. Neese, *WIREs Comput. Mol. Sci.* **2018**, *8*, e1327.

[24] a) J. P. Perdew, M. Ernzerhof, K. Burke, *J. Chem. Phys.* **1996**, *105*, 9982–9985; b) J. Tao, J. P. Perdew, V. N. Staroverov, G. E. Scuseria, *Phys. Rev.* **2003**, *91*, 146401.

[25] F. Weigend, R. Ahlrichs, *Phys. Chem. Chem. Phys.* **2005**, *7*, 3297–3305.

[26] R. S. Mulliken, *J. Chem. Phys.* **1956**, *23*, 1833–1840.

[27] P. Plessow, *J. Chem. Theory Comput.* **2013**, *9*, 1305–1310.

[28] P. J. Davidson, D. H. Harris, M. F. Lappert, *J. Chem. Soc. Dalton Trans.* **1976**, 2268–2274.

Manuscript received: May 20, 2021
Revised manuscript received: July 22, 2021
Accepted manuscript online: July 26, 2021

FULL PAPERS

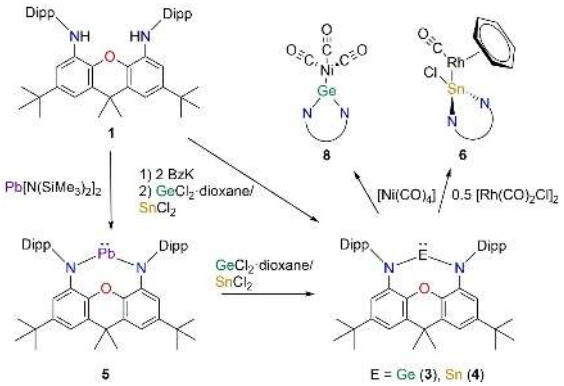

*F. Krämer, M. S. Luff, Prof. Dr. U. Radius, Prof. Dr. F. Weigend, Prof. Dr. F. Breher**

High NON! Different ways for the synthesis of NON-ligated *N*-heterocyclic germylene (**3**), stannylene (**4**) and plumbylene (**5**) were carried out. The title compounds were characterized using standard methods including X-ray diffraction. Initial investigations on the coordination behavior of **3**–**5** towards $[Rh(CO)_2Cl]_2$, $[W(CO)_6]$ and $[Ni(CO)_4]$ were performed. The σ-donor and π-acceptor properties were evaluated using density functional theory.